THE JOURNAL OF PHYSICAL CHEMISTRY C
A JOURNAL OF THE AMERICAN CHEMICAL SOCIETY

pubs.acs.org/JPCC

Article

Growth of van der Waals Halide Perovskites within the Interlayer Spacings of Mica

Saloni Pendse, Yang Hu, Ru Jia, Zhizhong Chen, Lifu Zhang, Skye Williams, Jie Jiang, Edwin Fohtung, and Jian Shi*

Cite This: *J. Phys. Chem. C* 2022, 126, 20074−20081

Read Online

ACCESS | Metrics & More | Article Recommendations | Supporting Information

ABSTRACT: Two-dimensional hybrid organic−inorganic perovskites (2D-HOIPs) have been extensively researched for use in solar cells as well as optoelectronic devices over the past few years. Controllable growth of single-crystalline 2D-HOIP thin films has been regarded as a key component for the development of high-performance end devices. Here, we report a solution-based method for the growth of 2D-HOIPs using muscovite mica as a van der Waals substrate that yields millimeter-scale perovskite flakes. Interestingly, the grown 2D-HOIP flakes lie embedded within the interlayer spacings of muscovite mica. We find that such 2D-HOIP flakes buried in mica demonstrate enhanced photostability in comparison to conventional 2D-HOIP flakes. Such liquid-phase growth in the interlayer spacings of van der Waals substrates opens a new avenue for developing novel material structures for designing optoelectronic devices.

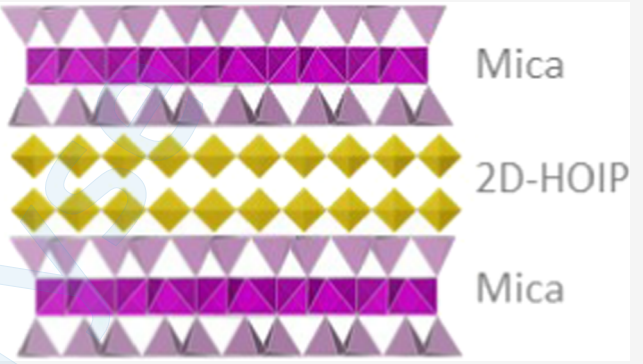

INTRODUCTION

Two-dimensional hybrid organic−inorganic perovskites (2D-HOIPs) have now been in the spotlight of research for the past few years owing to their excellent optoelectronic properties, wide tunability arising from compositional diversity, and improved resistance to moisture as compared to three-dimensional hybrid organic-inorganic perovskites (3D-HOIPs).[1,2] Considering these properties, several solar cells and optoelectronic devices based on polycrystalline 2D-HOIP films or 2D/3D-HOIP heterostructures with improved chemical stability and performance have been demonstrated.[3−5] However, to harness the full potential of these materials for applications such as optoelectronic devices as well as to explore their rich physics including ferroelectricity, Rashba splitting, and excitonic behavior, single-crystalline forms of 2D- HOIPs are a prerequisite.[6−15] Ultimately, for easy integration into devices, 2D-HOIPs in the form of single-crystalline thin films are highly desired. While bulk single crystals of 2D-HOIPs have been primarily obtained via solution growth in *N*,*N*-dimethylformamide, γ-butyrolactone, or water[11−14] and thin flakes or wires have been grown via specialized techniques such as drop casting,[10] cleaving,[13] templated growth,[7] and confined growth,[6,8] reports on facile growth of large 2D-HOIP flakes on various substrates[16] are less common. One method explored so far for such growth has been vapor-phase van der Waals (vdW) epitaxy.[17,18] As a growth technique, van der Waals epitaxy, where single-crystalline films or nanostructures are grown on 2D substrates such as graphene,[19] hexagonal boron nitride,[20] transition metal dichalcogenides,[21] or muscovite mica,[22−24] offers several advantages. These include a less stringent requirement for lattice matching, almost strain-free epilayers, reduced threading dislocations, and an abrupt interface free of cross-contamination or intermixing.[24] However, van der Waals epitaxy is typically carried out in the vapor phase via techniques like physical vapor deposition,[22] chemical vapor deposition,[19,20] or pulsed laser deposition.[24] This is in contrast with the existing knowledge base about growth of 2D-HOIPs that are mostly grown via solution-based techniques. In this work, we attempt to grow 2D-HOIPs on muscovite mica substrates using a solution-based approach.

MATERIALS AND METHODS

Materials. Butylamine ($CH_3(CH_2)_3NH_2$, 99.5%), lead iodide powder (PbI_2, 99%), hydroiodic acid (HI, ≥47%, ≤1.5% hypophosphorous acid as a stabilizer), (S)-(−)-1-(1-naphthyl)ethylamine ($C_{10}H_7CH(CH_3)NH_2$, ≥99%), lead bromide powder ($PbBr_2$, 99%), hydrobromic acid (HBr, 48%) were purchased from Sigma Aldrich. Grade V-5 muscovite mica

Received: September 6, 2022
Revised: October 22, 2022
Published: November 16, 2022

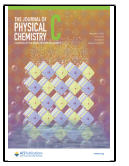

https://doi.org/10.1021/acs.jpcc.2c06379
J. Phys. Chem. C 2022, 126, 20074−20081

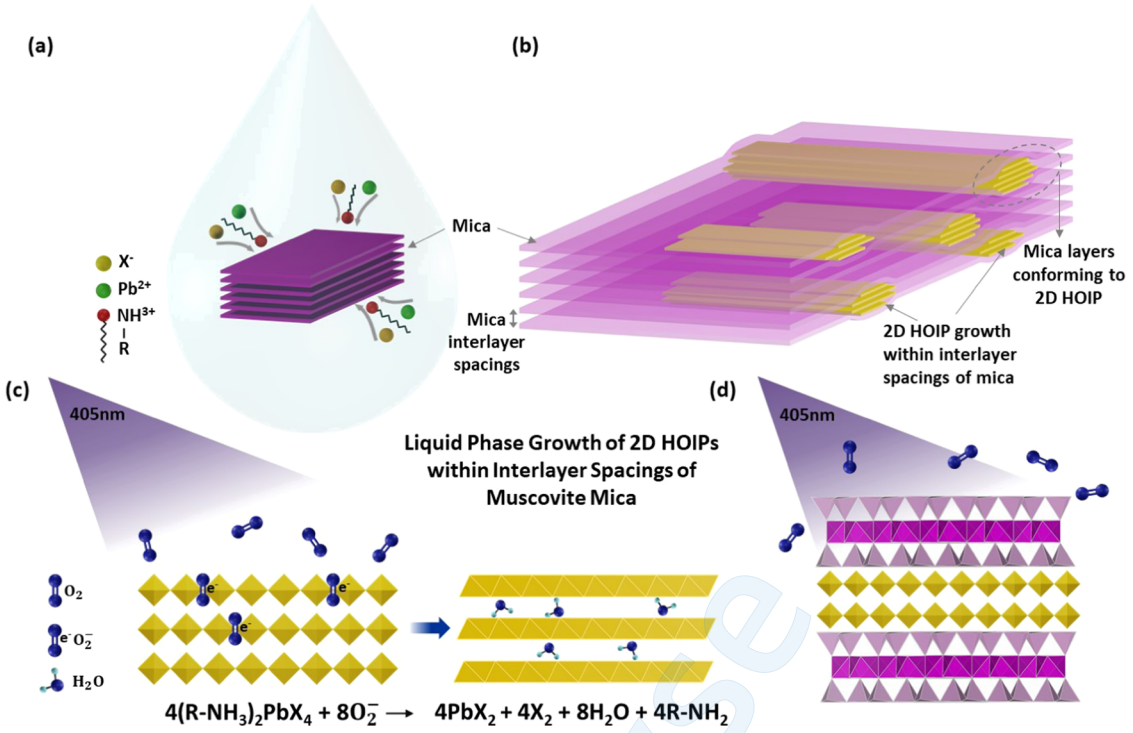

Figure 1. Schematic illustration of the growth of 2D hybrid organic−inorganic perovskites (HOIPs) in the interlayer spacings of muscovite mica. (a) Schematic illustration of ions migrating to the interlayer spacings of muscovite mica during solution-based growth of 2D-HOIPs on van der Waals mica. (b) Resultant growth of 2D-HOIPs in the interlayer spacings of the mica substrate with perovskite flakes distributed along the in-plane as well as the out-of-plane direction of mica. (c) Photodegradation pathway of a 2D-HOIP: (i) absorption of ambient oxygen, (ii) formation of superoxide (O_2^-) species due to its reaction with photogenerated electrons, and (iii) conversion to the PbX_2 form. (d) Enhanced photostability of 2D-HOIPs grown within the interlayer spacings of van der Waals mica by liquid-phase growth.

substrates with the (001) face exposed were purchased from SPI Supplies.

$(BA)_2PbI_4$ Growth. As a precursor for $(BA)_2PbI_4$ growth, *n*-butylammonium iodide (n-$CH_3(CH_2)_3NH_3I$) was first synthesized by adding a stoichiometric quantity of HI dropwise to $CH_3(CH_2)_3NH_2$ in an ice bath. In a separate vial, PbI_2 was dissolved in HI by stirring while heating to 120 °C. Once PbI_2 had dissolved in HI, stacks of freshly exfoliated muscovite mica were added to the solution. This was followed by the addition of a stoichiometric quantity of n-$CH_3(CH_2)_3NH_3I$ leading to initial formation of orange precipitates that quickly dissolved at 120 °C. Once the precipitates had dissolved, temperature of the solution along with the mica substrates was maintained at 90 °C for 0−4 h and then 60 °C for 0−9 h. Muscovite mica sheets with $(BA)_2PbI_4$ flakes growing within the interlayer spacings were then removed from the vial and dried at 50 °C.

$(NEA)_2PbBr_4$ Growth. The growth process was similar to that followed for growth of bulk $(NEA)_2PbBr_4$ crystals.[25] Stoichiometric quantities of $C_{10}H_7CH(CH_3)NH_2$, HBr, and $PbBr_2$ were added to deionized water along with stacks of muscovite mica. The solution was sealed in a vial at 95 °C followed by slow cooling over a period of 12 h. Muscovite mica sheets with $(NEA)_2PbBr_4$ flakes growing within the interlayer spacings were then removed from the vial and dried at 50 °C.

Characterization. The resulting 2D-HOIP flakes grown within the interlayer spacings of mica were studied and imaged under an optical microscope (Ti-S Nikon inverted microscope) either before or after the exfoliation of overlying mica layers. Structural characterization of the 2D-HOIP/muscovite mica assembly was done using a Panalytical X'pert PRO MPD system. Photoluminescence (PL) properties of the 2D-HOIP flakes were studied using a customized system consisting of a Picoquant 405 nm pulsed diode laser, a Nikon Eclipse Ti-S inverted optical microscope, a Thorlabs 4 Megapixel Monochrome Scientific CCD Camera, and a Princeton Instruments SP-2358 spectrograph. To collect temperature-dependent PL spectra, an INSTEC HCS302 temperature stage was used. Samples were glued to the stage with silver paste, and PL spectra were collected by loading the stage onto the optical microscope. A temperature range of −140 to 20 °C was scanned in intervals of 20 °C. The laser intensity was ∼2 mW. Photocurrent measurements of the 2D-HOIP flakes were carried out by preparing two terminal devices using silver paste. For flakes growing within interlayer mica spacings, the devices were prepared by adding drops of silver paste at mica edges. The silver paste flowed into the interlayer spacings to establish contact across the 2D-HOIP flakes. A 3.28 mW/cm^2 405 nm laser served as the illumination source, and photocurrent was measured using a potentiostat (Autolab PGSTAT302N).

RESULTS AND DISCUSSION

By adding muscovite mica to the growth solution, we show that 2D-HOIPs can be grown on top and, more interestingly, within the interlayer van der Waals spacings of muscovite mica. This is illustrated schematically in Figure 1a,b, where 2D-HOIP flakes of varying size and thickness are shown growing between individual sheets of a mica substrate and are distributed along the in-plane as well as the out-of-plane direction of mica. We expect that the muscovite mica surrounding the 2D-HOIP flakes grown within its interlayer spacings could help overcome the instability exhibited by HOIPs under illumination. Such photoinstability has been previously studied in 3D- as well as 2D-

https://doi.org/10.1021/acs.jpcc.2c06379
J. Phys. Chem. C 2022, 126, 20074−20081

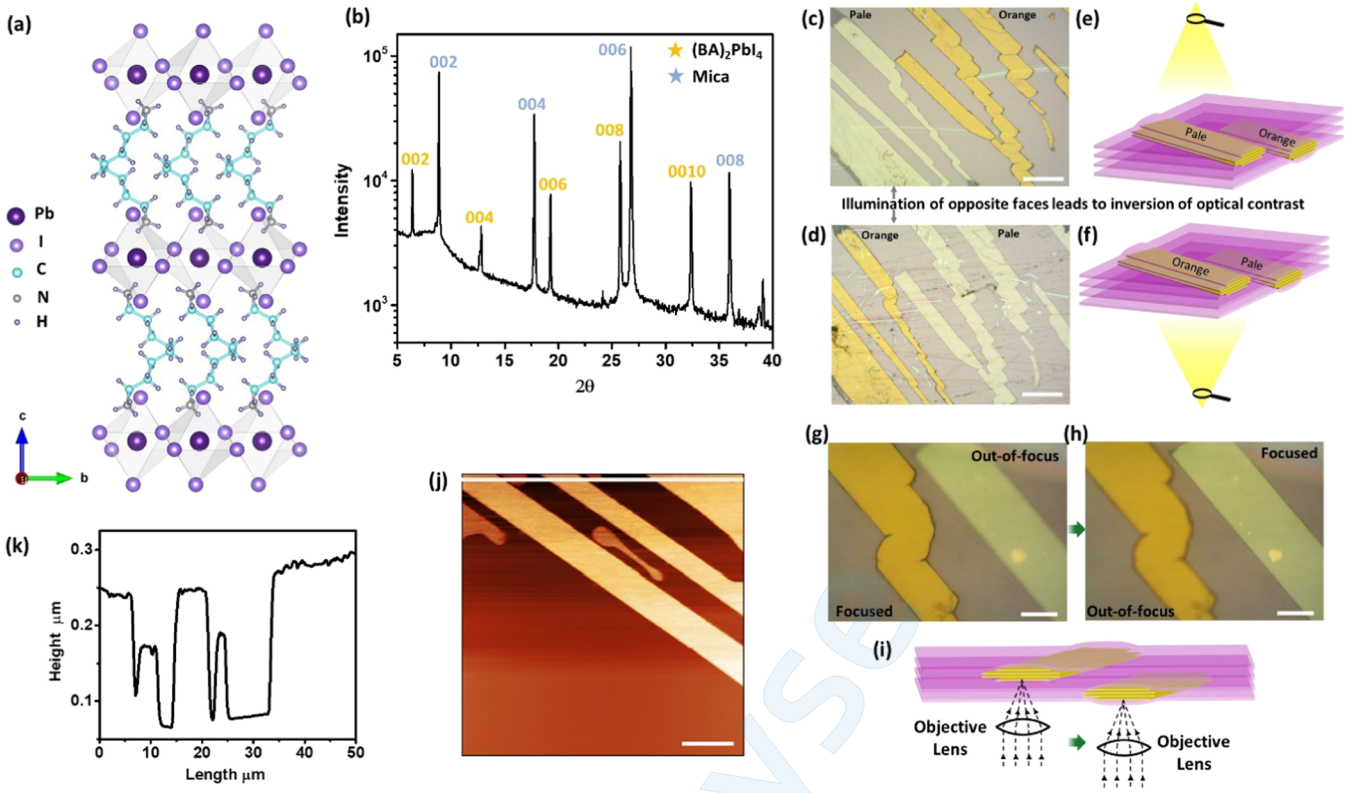

Figure 2. Growth of butylammonium lead iodide $(BA)_2PbI_4$ in the interlayer spacings of muscovite mica. (a) Polyhedron model of the $(BA)_2PbI_4$ crystal structure. Pb−I octahedra are shown in light gray separated by butylamine ligands. (b) Representative XRD scan of a $(BA)_2PbI_4$/mica stack. (c,d) Optical images of epitaxial $(BA)_2PbI_4$ flakes grown within the interlayer spacings of mica. Scale bar is 200 μm. Flakes are positioned at different depths along the out-of-plane direction of mica and those closer to the light source appear pale in color while those farther from the light source appear brighter orange in color. This leads to an inversion of optical contrast of flakes shown in (c) and (d) when illuminated from opposite sides as illustrated in (e) and (f). (g−h) Optical images highlighting the distribution of $(BA)_2PbI_4$ flakes along the out-of-plane direction of mica. Scale bar is 50 μm. (g) Objective of the microscope is adjusted to focus on the flake lying deeper within the mica stack. (h) Objective is repositioned to bring the lighter-colored flake lying closer to the light source into focus. (i) Schematic illustration of objective repositioning in (g, h). (j) AFM image of $(BA)_2PbI_4$ flakes after 10 min of growth time during liquid-phase van der Waals growth. (k) Line profile of the line highlighted at top of the AFM image.

HOIPs.[26−29] For example, a common degradation pathway for HOIPs is the reaction of photogenerated electrons with atmospheric oxygen to generate superoxide species (O_2^-) that aid in the conversion of the halide perovskite to its corresponding lead halide form as shown in Figure 1c for a $(R\text{-}NH_3)_2PbX_4$ Ruddlesden−Popper halide perovskite. It is expected that the muscovite mica surrounding the 2D-HOIP flakes grown within its interlayer spacings could act as an effective barrier against oxygen as shown in Figure 1d, thus enabling more reliable optical and optoelectronic characterization of the grown 2D-HOIPs.

We start with a model material butylammonium lead iodide ($(CH_3(CH_2)_3NH_3)_2PbI_4$), ($(BA)_2PbI_4$), a Ruddlesden−Popper (RP) halide perovskite ($(CH_3(CH_2)_3NH_3)_2A_{n-1}B_nPbX_{3n+1}$ with $n = 1$) to demonstrate the solution-based growth of 2D-HOIPs within the interlayer spacings of van der Waals mica. The mica substrate is typically a few tens of micrometers to a few hundreds of micrometers in thickness. We compare the photostability of $(BA)_2PbI_4$ flakes growing within the mica interlayer spacings with that of exposed $(BA)_2PbI_4$ flakes via photoluminescence and photoconductivity measurements. Furthermore, to demonstrate the versatility of this method for growth of 2D-HOIPs, we also grow flakes of 1-(1-naphthyl)-ethylammonium lead bromide ($(C_{10}H_7CH(CH_3)NH_3)_2PbBr_4$/$(NEA)_2PbBr_4$), a chiral RP 2D-HOIP ($(C_{10}H_7CH(CH_3)NH_3)_2A_{n-1}B_nPbX_{3n+1}$ with $n = 1$), in the interlayer spacings of mica.

Solution synthesis of $(BA)_2PbI_4$ was carried out as follows.[30] First, PbI_2 was dissolved in aqueous HI by heating to boiling followed by the addition of freshly cleaved stacks of mica to the vial. A stoichiometric quantity of $n\text{-}CH_3(CH_2)_3NH_3I$ was then added to this solution, and after the dissolution of the resulting orange precipitates under boiling, the solution was cooled in steps − first to 90 °C, where it was held for a duration varying from 0 to 4 h, followed by further cooling to 60 °C, where it was held for 0 to 9 h. Changing the growth time allowed tuning of the growth dimensions. The results from growth of $(BA)_2PbI_4$ within the mica interlayer spacings are presented in Figure 2. The crystal structure of the RP-phase $(BA)_2PbI_4$ shown in Figure 2a and Figure 2b shows a typical XRD scan of $(BA)_2PbI_4$ flakes grown within mica. Peaks corresponding to (0 0 2n) planes of $(BA)_2PbI_4$ can be clearly observed along with (0 0 2n) peaks of the muscovite mica substrate. Figure 2c−i shows optical microscopy images and corresponding schematics that illustrate the growth of $(BA)_2PbI_4$ flakes in the interlayer van der Waals spacings of a muscovite mica substrate. The difference in optical contrast between the two flakes shown in Figure 2c is a result of the position of each of these flakes at different depths along the out-of-plane direction of the mica substrate. The flake closer to the light source during imaging appears pale in color, while the flake buried at a deeper van der Waals spacing in mica appears

https://doi.org/10.1021/acs.jpcc.2c06379
J. Phys. Chem. C 2022, 126, 20074−20081

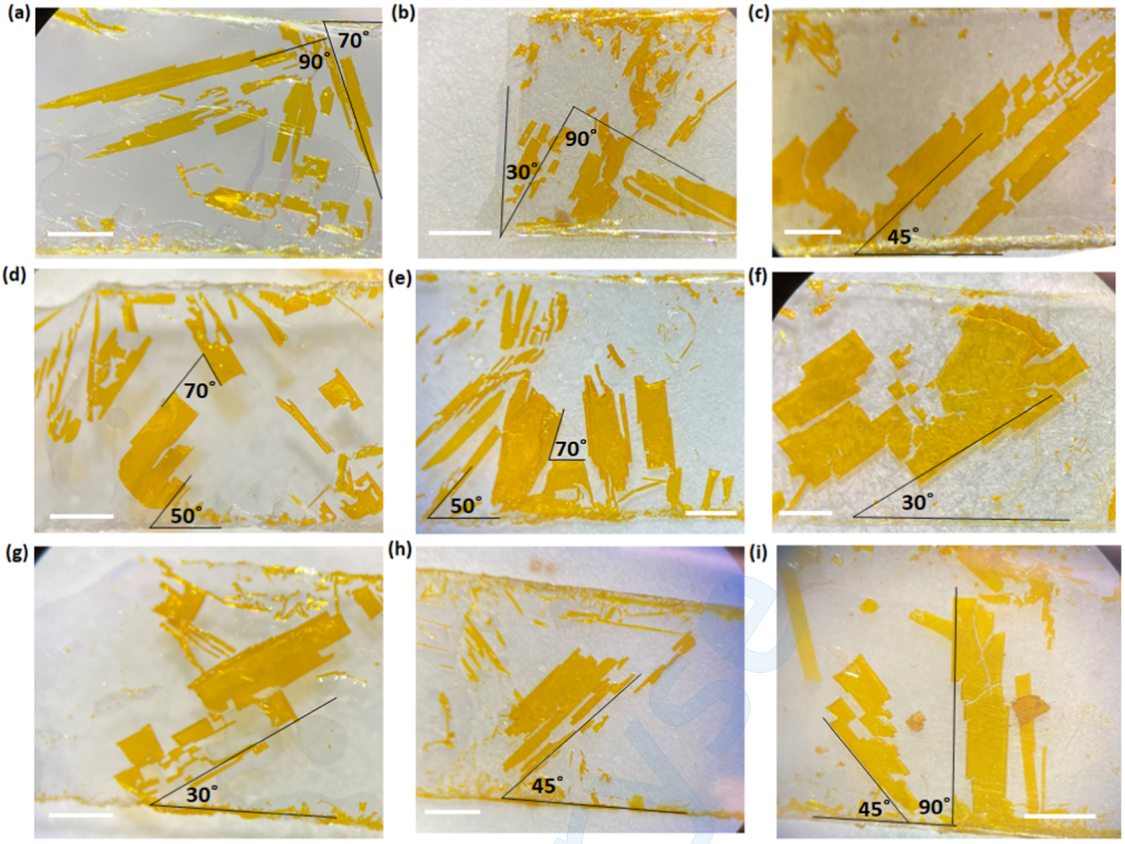

Figure 3. Photographs of $(BA)_2PbI_4$ flakes grown within the interlayer spacings of muscovite mica. Growth of $(BA)_2PbI_4$ flakes originates at the edges progressing inward with increasing growth time. Orientations of the $(BA)_2PbI_4$ flakes with respect to the edges of the mica substrate are highlighted above. All scale bars correspond to 1 mm in length.

bright orange in color. Figure 2c,d shows optical images of the same area of growth captured by illuminating opposite faces of the mica substrate as illustrated schematically in Figure 2e,f. The inversion of optical contrast of flakes between Figure 2c,d highlights the growth of $(BA)_2PbI_4$ flakes in interlayer van der Waals spacings distributed along the out-of-plane direction of mica. This is further explained in Figure 2g,h which provides a magnified view of the flakes shown in Figure 2c,d. In Figure 2g, the objective of the optical microscope is positioned so as to bring the flake lying at a deeper interlayer spacing into focus while the lighter-colored flake closer to the light source moves out of focus. In Figure 2h, the objective is repositioned bringing the lighter flake into focus. This is schematically illustrated in Figure 2i. Figure 2j–k show an Atomic Force Microscopy (AFM) image of BA_2PbI_4 flakes arrested in the early stages of growth (growth time = 10 min) and having a thickness of a few hundred nanometers. AFM samples were prepared by exfoliating sheets of mica until $(BA)_2PbI_4$ flakes were exposed at the surface. The thickness of the growing $(BA)_2PbI_4$ flakes can be varied from a few hundred nanometers to a few hundred micrometers by controlling the growth time. It is worth noting that although the interlayer bonds of mica are broken at growth sites of the $(BA)_2PbI_4$ flakes, the large lateral dimensions of mica allow the majority of interlayer bonds to remain intact causing the mica layers to conform to the growing $(BA)_2PbI_4$ flakes without exfoliation of the mica substrate. As such, the $(BA)_2PbI_4$ flakes remain protected within the surrounding mica layers.

Figure 3 presents the observation of millimeter-scale $(BA)_2PbI_4$ flakes grown within the interlayer spacings of muscovite mica. These flakes are commonly observed when the temperature of the growth solution is held at 90 °C for 4 h and then at 60 °C for 8 h. We studied orientations of the grown flakes with respect to muscovite mica substrates but did not find any consistent orientation relations, indicating the absence of epitaxy.

The intriguing growth of 2D-HOIP flakes in the van der Waals spacings of mica substrates has not been reported before. It has been established that due to strong electrostatic interactions, muscovite mica does not swell in aqueous solutions. This hinders intercalation and ion exchange reactions with K^+ ions of the muscovite.[31−34] Although exchange of organic ions and surfactants with K^+ ions has been demonstrated, the process is nontrivial, requires large surface areas with mica in a powder form, and is often limited to the exposed surface of muscovite.[31−33] Hence, it cannot directly explain the observed growth of $(BA)_2PbI_4$ in the interlayer spacings of large substrates of mica. However, it is known that liquids can enter the interlayer spacings of mica from its edges due to capillarity effects.[35,36] Such penetration of the growth solution into the interlayer spacings of mica, possibly aided by defects and cracks along the edges, can open up possibilities of ion exchange and cooling of the growth solution can promote crystallization of $(BA)_2PbI_4$ in pockets extending inward from the edges. This is supported by the general growth pattern of $(BA)_2PbI_4$ flakes shown in Figure 3, where a larger concentration of flakes is seen near mica edges, with growth progressing inward. An initiation of crystallization can promote further diffusion of precursors to the growth site leading to increasing thickness of the growing flake and hence widening of the interlayer spacing at the edges.

https://doi.org/10.1021/acs.jpcc.2c06379
J. Phys. Chem. C 2022, 126, 20074−20081

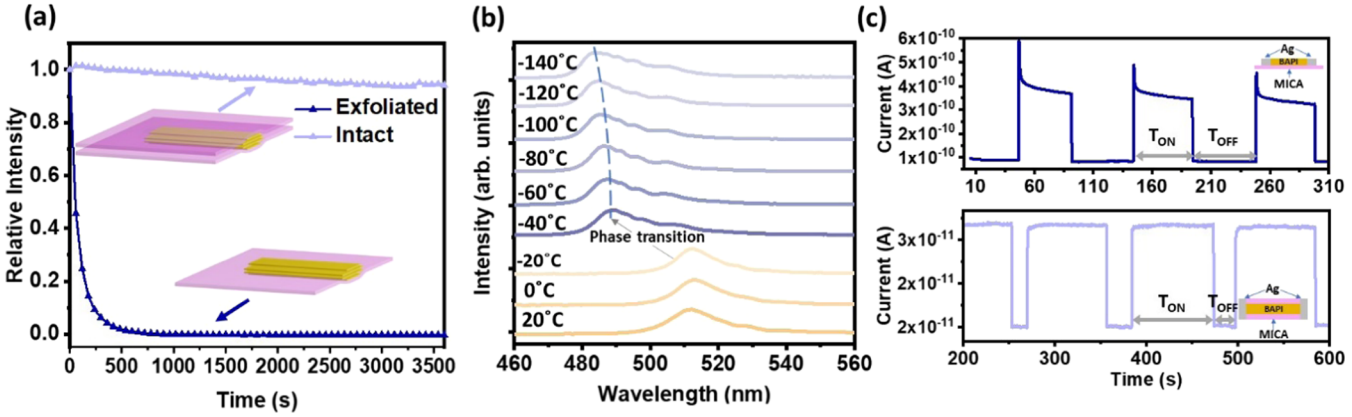

Figure 4. Photoluminescence (PL) and photoconductivity measurements of $(BA)_2PbI_4$ flakes embedded in mica and exposed to ambient air. (a) A comparative study of decay of PL intensity over time. (b) Temperature-dependent PL properties of a $(BA)_2PbI_4$ flake embedded in mica. (c) Comparative photoconductivity measurements for $(BA)_2PbI_4$ flakes growing within the interlayer spacings of mica (bottom panel) and $(BA)_2PbI_4$ flakes exposed to the atmosphere (top panel).

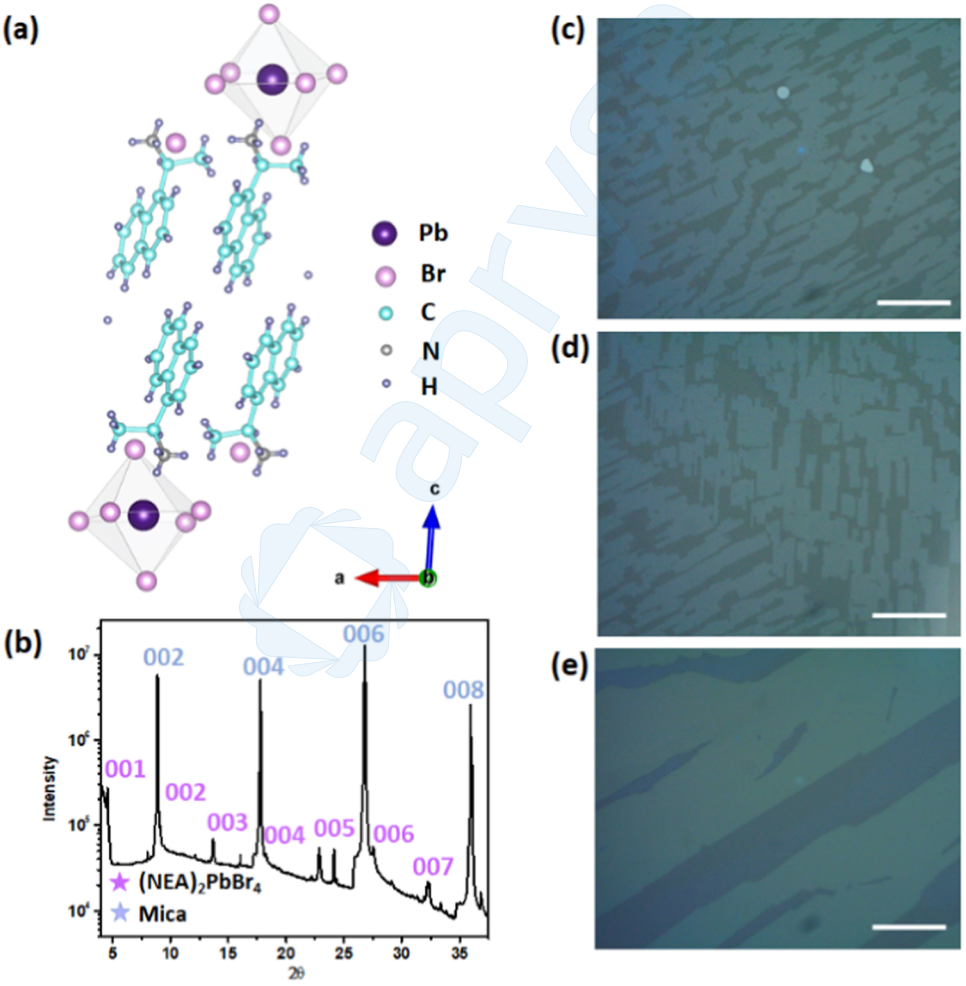

Figure 5. Growth of 1-(1-naphthylethylammonium) lead bromide $(NEA)_2PbBr_4$ in the interlayer spacings of muscovite mica. (a) Polyhedron model of the $(NEA)_2PbI_4$ crystal structure. Pb−Br octahedra are shown in light gray separated by naphthylethylamine ligands. (b) Representative XRD scan of a $(NEA)_2PbBr_4$/mica stack. (c−e) Optical images of $(NEA)_2PbBr_4$ growth within the interlayer spacings of mica. The scale bar is 30 μm. Images were obtained after peeling off overlying layers of mica for better clarity.

Figure 4 presents a comparison of optoelectronic properties of $(BA)_2PbI_4$ flakes grown and left intact within the interlayer spacings of mica with those of flakes exposed to the air. Figure 4a shows that while the photoluminescence (PL) of exposed $(BA)_2PbI_4$ flakes decays rapidly due to degradation into PbI_2, the PL of flakes naturally embedded in mica decays much more slowly, despite the exposed flake having a larger thickness than the embedded flake (shown in Figure S1). Hence, it can be said

https://doi.org/10.1021/acs.jpcc.2c06379
J. Phys. Chem. C 2022, 126, 20074−20081

that mica serves as an effective barrier against atmospheric oxygen, inhibiting its reaction with photogenerated electrons to form superoxide species. As such, rapid degradation of the $(BA)_2PbI_4$ flake that usually proceeds as $4(R\text{-}NH_3)_2PbI_4 + 8\ O_2^- \rightarrow 4PbI_2 + 4I_2 + 8H_2O + 4R\text{-}NH_2$ is largely prevented, allowing for steady and more reliable optical characterization of the 2D-HOIP under atmospheric conditions. Figure 4b shows temperature-dependent PL properties of $(BA)_2PbI_4$ flakes embedded in the interlayer spacings of a mica substrate, exhibiting features that are well-documented in the literature.[17,37−39] As the $(BA)_2PbI_4$ flake and mica assembly is cooled below room temperature, a slight red shift of the PL peak (originally at 512 nm) is seen followed by an abrupt blue shift to 488 nm between −20 and −40 °C. This shift in PL peak position is attributed to a structural phase transition and is associated with a change in the molecular state of butylammonium chains. Further decrease in temperature is seen to cause a gradual blue shift in the PL peak. Figure 4c compares photoconductivity measurements of a $(BA)_2PbI_4$ flake present within an interlayer spacing of mica with those of an exposed $(BA)_2PbI_4$ flake. Two terminal devices were prepared by depositing silver paste on exposed flakes. To prepare similar devices with flakes embedded in mica spacings, drops of silver paste were added at the edges of the surrounding mica. This allowed the silver paste to penetrate the mica and contact the underlying $(BA)_2PbI_4$ flake as shown in the inset of Figure 4c. It can be seen that while the photocurrent rapidly depletes in an exposed flake, a steady photocurrent can be maintained in a flake kept intact within the interlayer spacing of mica, another evidence of the barrier against oxygen provided by the surrounding mica. Along with the improved photostability, $(BA)_2PbI_4$ flakes kept intact within the interlayer spacings of mica also exhibited enhanced moisture and thermal stability and could be stored under ambient conditions for several weeks without significant changes in appearance or optoelectronic performance. Hence, growth of 2D-HOIP flakes within the interlayer spacings of a mica substrate can serve as an effective design strategy to measure inherent optoelectronic properties of 2D-HOIPs without interference from atmospheric conditions and to enhance the stability of optoelectronic devices based on 2D-HOIPs.

To explore the versatility of such solution-based growth of 2D-HOIPs within the interlayer spacings of mica, we also attempted the growth of 1-(1-naphthylethylammonium) lead bromide ($(NEA)_2PbBr_4$) by this method. The process was similar to that followed for growth of $(BA)_2PbI_4$. Stoichiometric quantities of 1(1-naphtylethylamine), hydrobromic acid (HBr), and lead bromide ($PbBr_2$) were added to water and dissolved by heating. Freshly cleaved sheets of mica were then added to the vial, and flakes or films of $(NEA)_2PbBr_4$ were seen growing in the interlayers of mica. The results are presented in Figure 5. The crystal structure of the RP-phase $(NEA)_2PbBr_4$ shown in Figure 5a and Figure 5b shows a typical XRD scan of $(NEA)_2PbBr_4$ flakes grown within mica. Peaks corresponding to (0 0 n) planes of $(NEA)_2PbBr_4$ can be clearly observed along with (0 0 2n) peaks of the muscovite mica substrate. Optical images of $(NEA)_2PbBr_4$ growth within the interlayer spacings of mica are shown in Figure 5c−e. Due to the colorless appearance of $(NEA)_2PbBr_4$, optical images were captured after removing the overlying layers of mica for sake of clarity. Hence, it can be said that solution-based growth within the interlayer spacings of mica can be an effective technique to grow $(NEA)_2PbBr_4$ flakes and may also be explored for the growth of other 2D-HOIPs. The grown 2D-HOIP flakes or films can be used as is, surrounded by a natural mica barrier that results from this growth method or may also be exposed to the atmosphere for further analysis by the exfoliation of overlying mica sheets.

CONCLUSIONS

In summary, we demonstrated solution-based growth of $(BA)_2PbI_4$ and $(NEA)_2PbBr_4$ 2D-HOIPs within the interlayer spacings of muscovite mica. The flakes were distributed in the interlayer spacings along the in-plane as well as the out-of-plane directions of mica. The size of the grown flakes ranged from a few microns to a few millimeters depending on the 2D-HOIPs being grown as well as the growth time. Properties such as PL and photoconductivity of the flakes were studied both with the natural barrier of mica and after exposure to the atmosphere by the exfoliation of overlying sheets of mica. It was seen that 2D-HOIP flakes grown and kept intact within the interlayer spacings of mica exhibited more stable PL and photocurrent, pointing to the effectiveness of the surrounding mica as a barrier against atmospheric oxygen. The solution-based growth of 2D-HOIPs in the interlayer spacings of mica can be harnessed for developing more reliable optical and optoelectronic devices.

ASSOCIATED CONTENT

Supporting Information

The Supporting Information is available free of charge at https://pubs.acs.org/doi/10.1021/acs.jpcc.2c06379.

The file contains additional experimental details (Note 1 and Figure 1) and optical images of growth results (Figure 2) (PDF)

AUTHOR INFORMATION

Corresponding Author

Jian Shi − *Department of Materials Science and Engineering, Rensselaer Polytechnic Institute, Troy, New York 12180, United States; Center for Materials, Devices and Integrated Systems, Rensselaer Polytechnic Institute, Troy, New York 12180, United States;* orcid.org/0000-0003-2115-2225; Email: shij4@rpi.edu

Authors

Saloni Pendse − *Department of Materials Science and Engineering, Rensselaer Polytechnic Institute, Troy, New York 12180, United States*

Yang Hu − *Department of Materials Science and Engineering, Rensselaer Polytechnic Institute, Troy, New York 12180, United States*

Ru Jia − *Department of Materials Science and Engineering, Rensselaer Polytechnic Institute, Troy, New York 12180, United States*

Zhizhong Chen − *Department of Materials Science and Engineering, Rensselaer Polytechnic Institute, Troy, New York 12180, United States*

Lifu Zhang − *Department of Materials Science and Engineering, Rensselaer Polytechnic Institute, Troy, New York 12180, United States*

Skye Williams − *Department of Materials Science and Engineering, Rensselaer Polytechnic Institute, Troy, New York 12180, United States*

Jie Jiang − *Department of Materials Science and Engineering, Rensselaer Polytechnic Institute, Troy, New York 12180, United States*

https://doi.org/10.1021/acs.jpcc.2c06379
J. Phys. Chem. C 2022, 126, 20074−20081

Edwin Fohtung − *Department of Materials Science and Engineering, Rensselaer Polytechnic Institute, Troy, New York 12180, United States; Department of Physics, Applied Physics and Astronomy, Rensselaer Polytechnic Institute, Troy, New York 12180, United States*

Complete contact information is available at: https://pubs.acs.org/10.1021/acs.jpcc.2c06379

Notes

The authors declare no competing financial interest.

■ ACKNOWLEDGMENTS

The authors acknowledge the New York State's Empire State Development's Division of Science, Technology and Innovation through Focus Center Contract C180117. They also acknowledge support from the US National Science Foundation under award numbers 2024972 and 2031692. They thank Prof. Gwo-Ching Wang for the use of the AFM in her laboratory.

■ REFERENCES

(1) Mao, L.; Stoumpos, C. C.; Kanatzidis, M. G. Two-Dimensional Hybrid Halide Perovskites: Principles and Promises. *J. Am. Chem. Soc.* **2019**, *141*, 1171−1190.

(2) Grancini, G.; Nazeeruddin, M. K. Dimensional Tailoring of Hybrid Perovskites for Photovoltaics. *Nat. Rev. Mater.* **2019**, *4*, 4−22.

(3) Grancini, G.; Roldán-Carmona, C.; Zimmermann, I.; Mosconi, E.; Lee, X.; Martineau, D.; Narbey, S.; Oswald, F.; De Angelis, F.; Graetzel, M.; Nazeeruddin, M. K. One-Year Stable Perovskite Solar Cells by 2D/3D Interface Engineering. *Nat. Commun.* **2017**, *8*, No. 15684.

(4) Liu, Y.; Akin, S.; Pan, L.; Uchida, R.; Arora, N.; Milić, J. V.; Hinderhofer, A.; Schreiber, F.; Uhl, A. R.; Zakeeruddin, S. M.; Hagfeldt, A.; Ibrahim Dar, M.; Grätzel, M. Ultrahydrophobic 3D/2D Fluoroarene Bilayer-Based Water-Resistant Perovskite Solar Cells with Efficiencies Exceeding 22%. *Sci. Adv.* **2019**, *5*, No. eaaw2543.

(5) Chen, S.; Shi, G. Two-Dimensional Materials for Halide Perovskite-Based Optoelectronic Devices. *Adv. Mater.* **2017**, *29*, No. 1605448.

(6) Liu, Y.; Zhang, Y.; Yang, Z.; Ye, H.; Feng, J.; Xu, Z.; Zhang, X.; Munir, R.; Liu, J.; Zuo, P.; et al. Multi-Inch Single-Crystalline Perovskite Membrane for High-Detectivity Flexible Photosensors. *Nat. Commun.* **2018**, *9*, No. 5302.

(7) Feng, J.; Gong, C.; Gao, H.; Wen, W.; Gong, Y.; Jiang, X.; Zhang, B.; Wu, Y.; Wu, Y.; Fu, H.; Jiang, L.; Zhang, X. Single-Crystalline Layered Metal-Halide Perovskite Nanowires for Ultrasensitive Photodetectors. *Nat. Electron.* **2018**, *1*, 404−410.

(8) Ding, R.; Lyu, Y.; Wu, Z.; Guo, F.; Io, W. F.; Pang, S. Y.; Zhao, Y.; Mao, J.; Wong, M. C.; Hao, J. Effective Piezo-Phototronic Enhancement of Flexible Photodetectors Based on 2D Hybrid Perovskite Ferroelectric Single-Crystalline Thin-Films. *Adv. Mater.* **2021**, *33*, No. 2101263.

(9) Gurioli, M.; Wang, Z.; Rastelli, A.; Kuroda, T.; Sanguinetti, S. Droplet Epitaxy of Semiconductor Nanostructures for Quantum Photonic Devices. *Nat. Mater.* **2019**, *18*, 799−810.

(10) Dou, L.; Wong, A. B.; Yu, Y.; Lai, M.; Kornienko, N.; Eaton, S. W.; Fu, A.; Bischak, C. G.; Ma, J.; Ding, T.; et al. Atomically Thin Two-Dimensional Organic-Inorganic Hybrid Perovskites. *Science* **2015**, *349*, 1518−1521.

(11) Liu, X.; Chanana, A.; Huynh, U.; Xue, F.; Haney, P.; Blair, S.; Jiang, X.; Vardeny, Z. V. Circular Photogalvanic Spectroscopy of Rashba Splitting in 2D Hybrid Organic−Inorganic Perovskite Multiple Quantum Wells. *Nat. Commun.* **2020**, *11*, No. 323.

(12) Park, I. H.; Zhang, Q.; Kwon, K. C.; Zhu, Z.; Yu, W.; Leng, K.; Giovanni, D.; Choi, H. S.; Abdelwahab, I.; Xu, Q. H.; et al. Ferroelectricity and Rashba Effect in a Two-Dimensional Dion-Jacobson Hybrid Organic-Inorganic Perovskite. *J. Am. Chem. Soc.* **2019**, *141*, 15972−15976.

(13) Li, L.; Sun, Z.; Wang, P.; Hu, W.; Wang, S.; Ji, C.; Hong, M.; Luo, J. Tailored Engineering of an Unusual (C4H9NH3)2(CH3NH3)-2Pb3Br10 Two-Dimensional Multilayered Perovskite Ferroelectric for a High-Performance Photodetector. *Angew. Chem., Int. Ed.* **2017**, *56*, 12150−12154.

(14) Liao, W. Q.; Zhang, Y.; Hu, C. L.; Mao, J. G.; Ye, H. Y.; Li, P. F.; Huang, S. D.; Xiong, R. G. A Lead-Halide Perovskite Molecular Ferroelectric Semiconductor. *Nat. Commun.* **2015**, *6*, No. 7338.

(15) Gao, Y.; Shi, E.; Deng, S.; Shiring, S. B.; Snaider, J. M.; Liang, C.; Yuan, B.; Song, R.; Janke, S. M.; Liebman-Peláez, A.; et al. Molecular Engineering of Organic−Inorganic Hybrid Perovskites Quantum Wells. *Nat. Chem.* **2019**, *11*, 1151−1157.

(16) Lei, Y.; Li, Y.; Lu, C.; Yan, Q.; Wu, Y.; Babbe, F.; Gong, H.; Zhang, S.; Zhou, J.; Wang, R.; et al. Perovskite Superlattices with Efficient Carrier Dynamics. *Nature* **2022**, *608*, 317−323.

(17) Chen, Z.; Wang, Y.; Sun, X.; Guo, Y.; Hu, Y.; Wertz, E.; Wang, X.; Gao, H.; Lu, T. M.; Shi, J. Van Der Waals Hybrid Perovskite of High Optical Quality by Chemical Vapor Deposition. *Adv. Opt. Mater.* **2017**, *5*, No. 1700373.

(18) Chen, Z.; Wang, Y.; Sun, X.; Xiang, Y.; Hu, Y.; Jiang, J.; Feng, J.; Sun, Y. Y.; Wang, X.; Wang, G. C.; et al. Remote Phononic Effects in Epitaxial Ruddlesden-Popper Halide Perovskites. *J. Phys. Chem. Lett.* **2018**, *9*, 6676−6682.

(19) Kim, J.; Bayram, C.; Park, H.; Cheng, C. W.; Dimitrakopoulos, C.; Ott, J. A.; Reuter, K. B.; Bedell, S. W.; Sadana, D. K. Principle of Direct van Der Waals Epitaxy of Single-Crystalline Films on Epitaxial Graphene. *Nat. Commun.* **2014**, *5*, No. 4836.

(20) Sundaram, S.; Li, X.; Halfaya, Y.; Ayari, T.; Patriarche, G.; Bishop, C.; Alam, S.; Gautier, S.; Voss, P. L.; Salvestrini, J. P.; et al. A. Large-Area van Der Waals Epitaxial Growth of Vertical III-Nitride Nanodevice Structures on Layered Boron Nitride. *Adv. Mater. Interfaces* **2019**, *6*, No. 1900207.

(21) Chen, K. H. M.; Lin, H. Y.; Yang, S. R.; Cheng, C. K.; Zhang, X. Q.; Cheng, C. M.; Lee, S. F.; Hsu, C. H.; Lee, Y. H.; Hong, M.; et al. Van Der Waals Epitaxy of Topological Insulator Bi2Se3 on Single Layer Transition Metal Dichalcogenide MoS2. *Appl. Phys. Lett.* **2017**, *111*, No. 083106.

(22) Wang, Q.; Safdar, M.; Xu, K.; Mirza, M.; Wang, Z.; He, J. Van Der Waals Epitaxy and Photoresponse of Hexagonal Tellurium Nanoplates on Flexible Mica Sheets. *ACS Nano* **2014**, *8*, 7497−7505.

(23) Jia, C.; Zhao, X.; Lai, Y. H.; Zhao, J.; Wang, P. C.; Liou, D. S.; Wang, P.; Liu, Z.; Zhang, W.; Chen, W.; et al. Highly Flexible, Robust, Stable and High Efficiency Perovskite Solar Cells Enabled by van Der Waals Epitaxy on Mica Substrate. *Nano Energy* **2019**, *60*, 476−484.

(24) Chu, Y.-H. Van Der Waals Oxide Heteroepitaxy. *npj Quantum Mater.* **2017**, *2*, 67.

(25) Jana, M. K.; Song, R.; Liu, H.; Khanal, D. R.; Janke, S. M.; Zhao, R.; Liu, C.; Valy Vardeny, Z.; Blum, V.; Mitzi, D. B. Organic-to-Inorganic Structural Chirality Transfer in a 2D Hybrid Perovskite and Impact on Rashba-Dresselhaus Spin-Orbit Coupling. *Nat. Commun.* **2020**, *11*, No. 4699.

(26) Aristidou, N.; Eames, C.; Sanchez-molina, I.; Bu, X.; Kosco, J.; Islam, M. S.; Haque, S. A. Fast Oxygen Diffusion and Iodide Defects Mediate Oxygen-Induced Degradation of Perovskite Solar Cells. *Nat. Commun.* **2017**, *8*, No. 15218.

(27) Aristidou, N.; Sanchez-molina, I.; Chotchuangchutchaval, T.; Brown, M.; Martinez, L.; Rath, T.; Haque, S. A. The Role of Oxygen in the Degradation of Methylammonium Lead Trihalide Perovskite Photoactive Layers. *Angew. Chem., Int. Ed.* **2015**, *54*, 8208−8212.

(28) Walsh, A.; Scanlon, D. O.; Chen, S.; Gong, X. G.; Wei, S. Self-Regulation Mechanism for Charged Point Defects in Hybrid. *Angew. Chem., Int. Ed.* **2015**, *54*, 1791−1794.

(29) Na Quan, L.; Ma, D.; Zhao, Y.; Voznyy, O.; Yuan, H.; Bladt, E.; Pan, J.; Arquer, F. P. G.; De; Sabatini, R.; Piontkowski, Z.; et al. Edge Stabilization in Reduced-Dimensional Perovskites. *Nat. Commun.* **2020**, *11*, No. 170.

(30) Stoumpos, C. C.; Cao, D. H.; Clark, D. J.; Young, J.; Rondinelli, J. M.; Jang, J. I.; Hupp, J. T.; Kanatzidis, M. G. Ruddlesden − Popper

Hybrid Lead Iodide Perovskite 2D Homologous Semiconductors. *Chem. Mater.* **2016**, *28*, 2852−2867.
(31) Weng-Lip, L.; Salleh, N. M.; Rahman, N.; Aqilah, A.; Bakhtiar, N. S. A. A.; Akil, H. M.; Zubir, S. A. Enhanced Intercalation of Organo-Muscovite Prepared via Hydrothermal Reaction at Low Temperature. *Bull. Mater. Sci.* **2019**, *42*, No. 242.
(32) Che Ismail, N. H.; Ahmad Bakhtiar, N. S. A.; Md Akil, H. Effects of Cetyltrimethylammonium Bromide (CTAB) on the Structural Characteristic of Non-Expandable Muscovite. *Mater. Chem. Phys.* **2017**, *196*, 324−332.
(33) Yu, X.; Zhao, L.; Gao, X.; Zhang, X.; Wu, N. The Intercalation of Cetyltrimethylammonium Cations into Muscovite by a Two-Step Process: I. The Ion Exchange of the Interlayer Cations in Muscovite with Li. *J. Solid. State. Chem.* **2006**, *179*, 1569−1574.
(34) Gaines, G. L. The Ion-Exchange Properties of Muscovite Mica. *J. Phys. Chem. a* **1957**, *61*, 1408−1413.
(35) Skow, M. L. *Mica - A Materials Survey, U.S. Department of Interior*, Bureau of Mines: Washington, 1962.
(36) Hansma, H. G. Possible Origin of Life between Mica Sheets. *J. Theor. Biol.* **2010**, *266*, 175−188.
(37) Lin, C. W.; Liu, F.; Chen, T. Y.; Lee, K. H.; Chang, C. K.; He, Y.; Leung, T. L.; Ng, A. M. C.; Hsu, C. H.; Popović, J.; et al. Structure-Dependent Photoluminescence in Low-Dimensional Ethylammonium, Propylammonium, and Butylammonium Lead Iodide Perovskites. *ACS Appl. Mater. Interfaces* **2020**, *12*, 5008−5016.
(38) Ni, L.; Huynh, U.; Cheminal, A.; Thomas, T. H.; Shivanna, R.; Hinrichsen, T. F.; Ahmad, S.; Sadhanala, A.; Rao, A. Real-Time Observation of Exciton-Phonon Coupling Dynamics in Self-Assembled Hybrid Perovskite Quantum Wells. *ACS Nano* **2017**, *11*, 10834−10843.
(39) Lemmerer, A.; Billing, D. G. Synthesis, Characterization and Phase Transitions of the Inorganic-Organic Layered Perovskite-Type Hybrids [(C NH 2n+1NH 3) 2PbI 4], n = 7, 8, 9 and 10. *Dalton Trans.* **2012**, *41*, 1146−1157.

https://doi.org/10.1021/acs.jpcc.2c06379
J. Phys. Chem. C 2022, 126, 20074−20081